

Original paper

NEW EMPIRICAL FORMULAE OF UNDERTOW VELOCITY ON MIXED AND GRAVEL BEACHES

Christos antoniadis

External Research Fellow in Port Engineering in Civil Engineering Department of Democritus University of Thrace, Xanthi, 67100, Greece

Received : February 3, 2013; Accepted: February 27, 2013

ABSTRACT

This paper reports a series of 3-dimensional physical model tests to measure cross-shore current data, generated by oblique wave attack, along gravel and mixed beaches with a uniform slope and a trench. Coastal managers and coastal engineers are beginning to give attention to gravel and mixed beaches due to the fact that they are two of the most effective natural sea defences. There is a need, from a scientific and coastal management perspective to have a deeper understanding of how gravel and mixed beaches operate. The studies described in this paper aim to investigate the behaviour of the undertow velocity on mixed and gravel beaches. Existing formulae have been used to predict the experimental results and new equations for predicting the undertow velocity under these conditions are proposed.

The new empirical formulae predict time- and depth-averaged undertow and are based on a nonlinear regression of a modification of the Grasmeyer's and Ruessink's model where the zones were divided based on the related distance of the point of interest and the breaking point. Verification with large-scale experiments showed that the new formulae predicted well the undertow velocities on mixed and gravel beach with trench and uniform slope.

Keywords: gravel, mixed beach, wave-induced currents, trench, wave breaking, undertow

***Correspondence:** Phone: +30- 6979708081; Fax: +30- 2541062939; E-mail: cantoniadis79@hotmail.com

INTRODUCTION

As the oblique waves break to the shoreline two mean currents are generated flowing parallel (long-shore currents) and straight normal (cross-shore currents) to the coast. These two mean currents can be considered as components of a continuum flow field from which the resulting wave-induced mean current structure is illustrated in Fig. 1 (Svendsen and Lorenz, 1989). These nearshore currents in combination with the stirring action of the waves are important for the sediment transport and therefore are significant factors in morphological changes. Consequently, they are of great importance for managers of coastal areas, coastal engineers and marine geologists (Visser, 1991).

Cross-shore currents are related to the mass compensation under breaking waves and

they are not constant over depth (Coastal Engineering Manual, 2003). The main characteristic of the cross-shore current is the existence of the two-dimensional circulation in the surf zone known as "undertow current", which flows in the seawards direction from the shoreline. This current is directed offshore on the bottom, balanced with the onshore flow of water carried by the breaking waves. Closer to the water surface the resulting current is in the onshore direction. The undertow current may be relatively strong, being almost 8% to 10% of the wave celerity ($\sqrt{g\lambda}$) near the bottom.

The undertow is the result of an imbalance between the excess momentum flux induced by the breaking wave, the mass flux of the carrier wave and the surface roller, concentrated on the surface layer between the wave crest and

trough, and the hydrostatic excess pressure caused by the local mean water level gradient (setup), which becomes predominant below wave trough level (Briand and Kamphuis, 1993).

The undertow can be considered as an explanation of bar formation (in the surf-zone, close to the wave breaking point) observed, under wide range of conditions, on beach profiles in the laboratory and in the field (Briand and Kamphuis, 1993; Svendsen, 1984a and Deigaard *et al.*, 1991).

The first quantitative analysis of the undertow was by Dyhr-Nielsen and Sorensen (1970). Furthermore, the undertow profile is solved by Dally and Dean (1984), Svendsen (1984a), Hansen and Svendsen (1984), Stive and Wind (1984), Svendsen *et al.* (1987) and Svendsen and Buhr Hansen (1988).

To extend our understanding within the coastal environment a 3-dimensional physical model (see

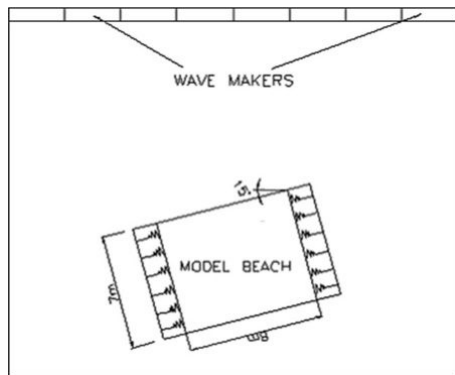


Fig.

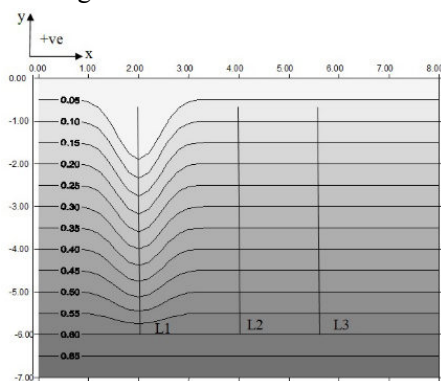


Fig. 3,

Table 1 and Table 2) was used to examine wave breaking formulae for obliquely incident waves on mixed and gravel beaches (Antoniadis, 2009).

MATERIALS AND METHODS

The Experiment

The experiments were carried out in the three-dimensional wave basin located at Franzius-Institute (Marienwerder), Hannover University. The experiments ran for nearly 70 days and were undertaken for a beach model which consisted at first of gravel sediment and secondly of mixed sediment. The beach model with dimensions of 8m x 7m x 0.7m was set up in the middle of the wave basin. It was open to the side from which the generated waves were approaching. The beach model was oriented in such a way that waves, generated by the wave paddle, were always approaching it with an angle of 15° (Fig.2). Beach bathymetry consisted of a uniform slope beach (straight-line parallel contour) and a trench (curved contour) with a width of 2m, as shown in Fig.3. The location and the dimensions of the trench in the physical model would not have any significant impact in the profile changes of the beach with the uniform slope.

Data Collection

The experiment comprised of ten tests, which were mainly focused on the wave current measurements across the gravel and mixed beach. The measurements of the wave driven current were carried out with an ADV. The measurements of currents started 30 minutes after the first wave was generated for both regular and random waves. These 30 minutes were sufficient to eliminate bed level changes during the measurements, which could influence the currents. At that point, an equilibrium state was reached, in which no sediments were moving. However, for the mixed beach, the sand was moved slightly after the 30 minutes period, without any sufficient influence in the measurements. The currents were measured, in time, at three cross-shore sections of the beach. The first was at the

2,

curved beach section and the other two at the straight beach section, for all three space directions V_x , V_y and V_z . These sections are shown as lines in Fig.3. Velocities V_x and V_y were considered positive when heading towards the positive direction of x and y axes (Fig.3), while the vertical velocity V_z was considered positive when heading upwards. The measurements had reached the maximum of -4.7m at y -direction due to the fact that the ADV can work only at submerged sections. Despite that, the number of current velocity measurements that was taken was satisfactory. Current velocity measurements were carried out at various levels along the z direction. At each level, the current velocity measurements were taken over a period of 60 seconds. Observations for regular waves started at the surface and deepened with a constant 5cm interval until the maximum point was reached. The maximum point was the point at which the ADV could take logical measurements, usually that was between 5 and 10cm above the bed level. The deepest point of measurement was 35cm below water surface.

The same procedure was followed for random waves but with a 10cm interval. The deepest point of measurement for random waves was 30cm below the water surface. This procedure allowed an estimate of the vertical structure of the time-averaged velocity and a more accurate determination of the depth-averaged current velocities. The depth-averaged current velocity V was determined as:

$$V = \frac{(V_{\text{surface}} + 2V_{\text{mid-depth}} + V_{\text{bottom}})}{4}$$

Data Analysis

The cross-shore currents, of each line and for each test, that measured from the experiments were analysed and can be observed at the Appendix A. The reverse flow can clearly be seen at all lines for all tests. Most of the measurement points were before the breaking point but close enough the undertow current to be observed. The undertow was represented (in Appendix A) by the seaward direction of the currents. Furthermore, at the trench, the seaward direction of the currents could represent rip currents, especially at Test 1 and

Test 2 where the highest wave conditions of the experiment occurred.

Rip currents are usually confused with the undertow. As the waves move to the shoreline produces setup. Because of the inclination of the water level, the setup water is essentially piled up against the shoreline in an unstable condition. If this unstable condition exists along a barred coast or along some of the steeper coasts, the setup produces seaward flowing currents that are rather narrow and that create circulation cells within the surf zone. These narrow currents are called rip currents.

When wind and waves push water towards the shore, the previous backwash is often pushed sideways by the oncoming waves. This water streams along the shoreline until it finds an exit back to the sea. The resulting rip current is usually narrow and located in a trench. In general, while a common misconception is that a rip occurring under the water, instead of on top — an undertow — is strong enough to drag people under the surface of the water; the current is actually strongest at the surface. In some areas, rip currents will persist during low-to moderate- energy wave conditions and then during high-energy wave conditions the rips will lose their definition and undertow will be primary mode of seaward return of water from unstable condition of setup.

Though, it has to be mentioned that at some locations, near the bed, the reverse current is replaced by a shoreward current. This behaviour of currents is carried out from Test 4 to Test 10 (especially with uniform slope "Lines 2 and Line 3"). The shoreward direction of these currents also affected the sediment transport as the sediment showed to be slightly moved shoreward at the locations influenced by these currents. The cross-shore current velocities of all tests, near the bed, are

presented at

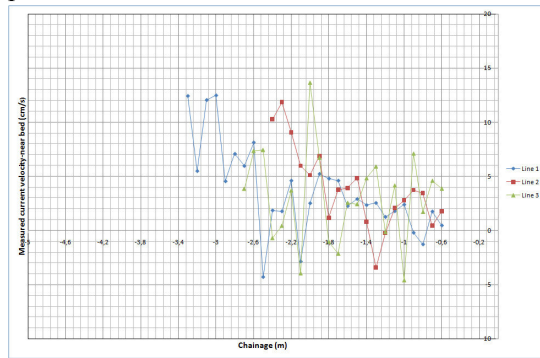


Fig. 4 to

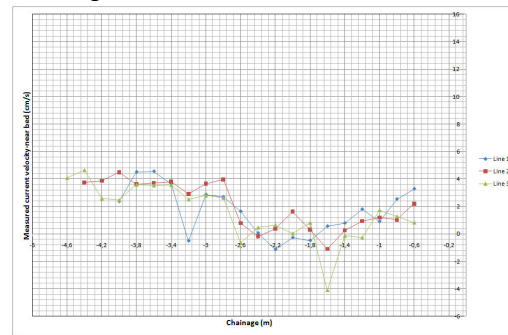


Fig. 4 to

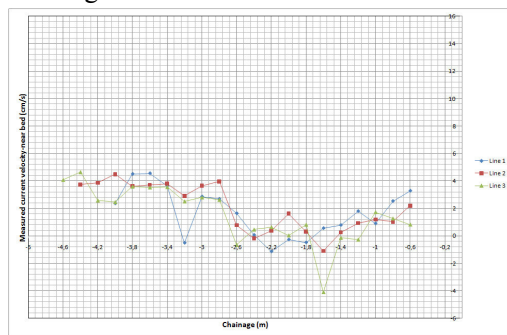


Fig. 13. In the y-direction, positive indicates seaward where negative indicates shoreward.

The cross-shore current velocity was expected to be very small, close to zero, near the bed. However, in

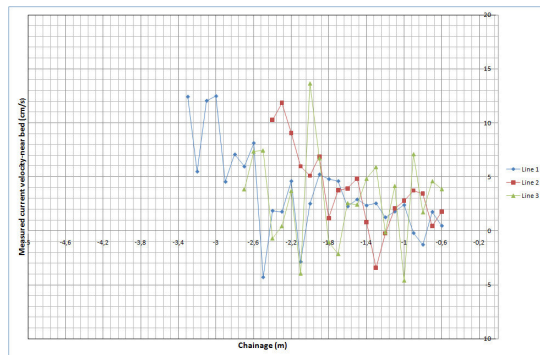


Fig. 13, velocities were not always zero or small. It was expected currents to have higher values close to the breaking point. However, during the tests, currents had relatively high values (for both shoreward and seaward directions) even before the breaking point. The shoreward currents had maximum value near to 5cm/s. The near bed cross-shore currents have shown an oscillating direction, from seaward to shoreward and from shoreward to seaward, along the cross-shore section of the beach.

Lara *et al.* (2002), showed how the undertow behaves over a highly permeable bed. They conducted an experimental study in a laboratory, showing the mean flow characteristics over impermeable and permeable beds. Their study discussed the differences between water surface envelopes and undertow for these cases. They showed that the effect of a permeable bed ($D_{50}=19$ and 39 mm) on the undertow is a change of the velocity profile, with the magnitude of undertow close to the seafloor reduced. This effect was more important in decreasing water depth and it was reduced for decreasing gravel size.

During Test 1 to Test 10, the sizes of D_{50} were 23mm and 12mm for gravel and mixed beach respectively, which are at the low range of the ones that were used in the experiments of Lara *et al.* (2002). The gravel beach is more permeable than the mixed beach, which sometimes tends to be impermeable. However, the undertow close to the bed was not only reduced but was increased and was replaced by a shoreward current even outside the surf zone. This shoreward current could cause suspended sediment to be moved landward. This behaviour of the undertow was more noticeable

at the tests with gravel beach. By comparing the magnitude of velocities between the gravel and mixed bed, it can be seen that the velocities were higher at the gravel bed where the D_{50} was also the highest. This is in agreement with the observation of Lara *et al.* (2002).

Nevertheless, the increase and even the change of direction of the velocities near the bed, especially in the gravel bed, can be due to the mechanism of bed-generated turbulence. Lara *et al.* (2002) stated that the gravel bed-generated turbulence characteristics depend on the gravel size and increasing gravel size results in an increase in the velocity gradient, which is the principal mechanism for the generation of larger-scale turbulence over the gravel bed. This mechanism of bed-generated turbulence has been noticed by Buffin-Bélanger *et al.* (2000) and Shvidchenko *et al.* (2001) over gravel bed rivers resulting in Reynolds stresses that have different signs, revealing different vortex orientation (Lara *et al.*, 2002).

In the surf zone, the turbulence can be related to the type of breaking because partly or even the whole mechanism for the generation of turbulence is induced to the breaking process. The characteristics of turbulence structure and undertow are different in spilling and plunging breakers. Turbulent kinetic energy is transported seaward under the spilling breaker. This is different from the plunging breaker where turbulent kinetic energy is transported landward (Ting and Kirby, 1994).

RESULTS AND DISCUSSION

Results

Comparison with other existing methods

In this section, a comparison is given with other existing formulations that calculate the time-averaged and depth-averaged undertow. Various authors have presented models for predicting cross-shore currents, especially undertow.

Kuriyama and Nakatsukasa (2000) developed a one-dimensional model which predicts the time- and depth- averaged undertow velocities. The model was calibrated with field data obtained over longshore bars at Hazaki Oceanographical Research Station

(HORS) and it predicted well the undertow over the longshore bars.

Grasmeijer and Ruessink (2003) presented a hydrodynamic model that can predict also the time-averaged cross-shore currents (undertow) in a parametric and probabilistic mode. The model was calibrated with laboratory and field experiments and it predicted well the undertow. Furthermore, Tajima and Madsen (2006) developed a near-shore current model based on Tajima and Madsen's (2002, 2003) wave and surface roller models. There was a generally good agreement of predicted the undertow velocity profiles by using the model.

Pedrozo-Acuna *et al.* (2006) presented an estimation of the value of the undertow velocity from a Boussinesq model by explicitly allowing for the higher velocity in the roller region of a breaking wave front (e.g. Madsen *et al.*, 1997). The value of undertow U_o was written as

$$U_o = \frac{M - c\delta}{\zeta + h - \delta}$$

(1)

where,

$$M = (h + \zeta) \left[\begin{array}{l} u_a + \left(\frac{1}{2} z_a^2 - \frac{1}{6} (\zeta^2 - \zeta h + h^2) \right) \nabla(\nabla u_a) + \\ \left(z_a + \frac{1}{2} (h - \zeta) \right) \nabla[\nabla(u_a)] \end{array} \right]$$

(2)

ζ is the free surface elevation, h is the local water depth, u_a is the reference horizontal velocity at the elevation given by z_a ($z_a = -0.531h$, Nwogu, 1993), c is the wave celerity and δ is the roller thickness. The roller contribution is minimal (Pedrozo-Acuna *et al.*, 2006).

The experimental data was compared with the models of Kuriyama and Nakatsukasa (2000) and Grasmeijer and Ruessink (2003). The model of Grasmeijer and Ruessink (2003) was used in parametric mode as its authors stated that it would give the same accuracy with a computationally quicker approach than the probabilistic mode. The calculation procedures of both models are presented in Appendix B and C.

Both models used the mass flux due to the wave motion and the mass flux due to the surface roller to estimate the undertow velocity. However, each of the models calculated these

mass fluxes in a different way. The model of Kuriyama and Nakatsukasa (2000) did not include the angle of incidence; however, in the comparison with the experimental results, it was included. At the model of Grasmeyer and Ruessink (2003), the procedure of calculating the roller area was not described. However, in the comparison with the experimental results, the roller area was presented and calculated twice based on the following two equations:

Engelund (1981) made a simple dynamic model of a hydraulic jump, which is based on the depth-integrated horizontal momentum equation and gives the local thickness of the surface roller. Engelund assumed that the boundary between surface roller and the water below is a straight line. Using an analogy between the velocity distribution in separated diffuser flow and in the hydraulic jump, it was argued that the angle θ between this boundary and the horizontal is about 10^0 . With accuracy within a few per cent the roller area obtained by the model of Engelund (1981) can be calculated as

$$A = \frac{H^2}{\tan \theta} \frac{H_1}{4} \quad (3)$$

Duncan (1981) has made measurements of rollers in waves that have been generated by a towed hydrofoil. Svendsen (1984b) approximated these results with the relation

$$A = 0.9H^2 \quad (4)$$

The graphical presentations of the comparison of the experimental undertow velocities results, for all Lines and all tests, with the two models are shown in

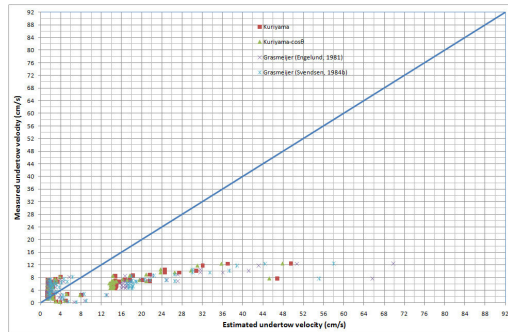


Fig 14 to

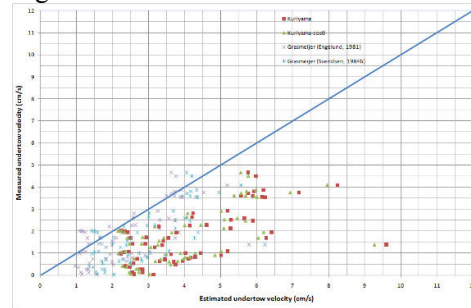


Fig 21 (the positive values represent the undertow velocities).

In

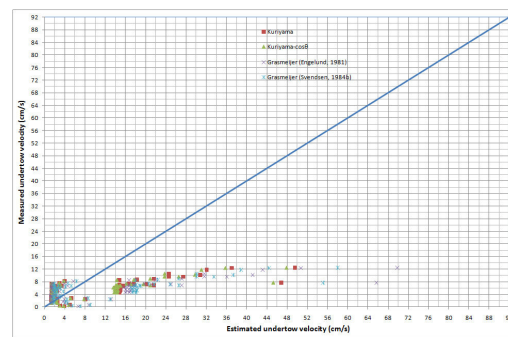


Fig 14 to

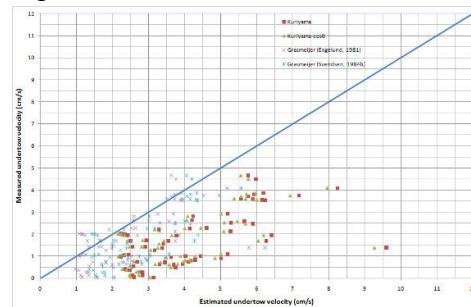


Fig. 21, Kuriyama and Nakatsukasa (2000) stated as “Kuriyama” and Grasmeyer and Ruessink (2003) as “Grasmeyer”. The two models, and their modifications, were not estimated as accurate as it was expected. However, they had a good correlation with the trench for random waves for both gravel and mixed beach. In general, they overestimated the values of undertow velocities for uniform slope in both regular and random wave conditions and for both gravel and mixed beach. In contrast with undertow velocities in uniform slope, undertow velocities in the trench were

generally underestimated by the models (except for gravel beach-regular waves).

The model of Kuriyama and Nakatsukasa (2000) with the inclusion of the angle of incidence, had better correlation than the other models, with uniform slope for regular wave conditions (with both mixed and gravel beach) and with trench for random wave conditions (with both mixed and gravel beach). In general, the correlations of this model (Kuriyama and Nakatsukasa, 2000) with the measured data were poor because it was initially developed and calibrated with the undertow velocities measured over longshore bars and it mainly has been applied on barred beaches.

The model of Grasmeyer and Ruessink (2003) in relation with the equation of Svendsen (1984b), had better correlation with the other models, with trench for regular wave conditions (with both mixed and gravel beach) and with uniform slope for random wave conditions (with gravel beach). The model of Grasmeyer and Ruessink (2003), with the use of relation of Engelund (1981), had better agreement than the others with uniform slope

for random wave conditions (with mixed beach). Despite that, this model (Grasmeyer and Ruessink, 2003) showed rather poor agreement with the measurements. The discrepancies may be caused by the use of linear wave theory to compute the mean mass transport associated with the organised wave motion in the model. As for this model (Grasmeyer and Ruessink, 2003) and the model of Kuriyama and Nakatsukasa (2000), it is needless to say that the predictive performance of the 2D model is poor for cases where 3D circulations are important.

New empirical equations

Based on a non-linear regression analysis, empirical relations have been generated in order to predict much more accurate the experimental results. These empirical relations are based on the results of the model Grasmeyer and Ruessink (2003). The non-linear regression has been fitted to the data and the proposed fits are shown by the following equations:

Regular Wave Conditions

For gravel beach (trench):

$$\frac{U}{u_{cb}} = -2278.898 + \frac{6829.806}{X} + 775.664A - \frac{6748.670}{X^2} - 87.836A^2 - 1563.506 \frac{A}{X} + \frac{2199.256}{X^3} + 3.224A^2 + 89.543 \frac{A^2}{X} + 776.899 \frac{A}{X^2} + AX$$

(5)

For gravel beach (uniform slope):

$$\frac{U}{u_{cb}} = 0.333 + 2.815 \ln(X) + 5.709 \ln(X)^2 - 19.254 \ln(X)^3 + 5.966 \ln(X)^4 - 0.906 \ln(X)^5 - 1.215A - 0.134A^2 + (4.4 \times 10^{-3})A^3 + (2.86 \times 10^{-4})A^4 - (2.729 \times 10^{-7})A^5 + AX$$

(6)

For mixed beach (trench):

$$\frac{U}{u_{cb}} = -160.807 + 19.584X - 11.530X^2 + 2.695X^3 - 0.304X^4 + 0.01268X^5 + \frac{1933.442}{A} - \frac{10066.792}{A^2} + \frac{25203.259}{A^3} - \frac{29766.799}{A^4} + \frac{13102.164}{A^5} + AX$$

(7)

For mixed beach (uniform slope):

$$\frac{U}{u_{cb}} = 0.135 + 1.015 \ln(X) - 1.044A + 38.768 \ln(X)^2 + 0.686A^2 - 11.093 \ln(X)A + 1.734 \ln(X)^3 - 0.13A^3 + 1.902 \ln(X)A^2 - 8.27 \ln(X)^2A + AX$$

(8)

Random Wave Conditions

For gravel beach (trench):

$$\frac{U}{u_{cb}} = -53.142 + 127.971X - 112.891X^2 + 49.620X^3 - 11.038X^4 + 0.977X^5 - 1.873A + 0.0282A^2 - 0.016A^3 - 0.00124A^4 + 0.000155A^5 + AX \quad (9)$$

For gravel beach (uniform slope):

$$\frac{U}{u_{cb}} = 592.981 - \frac{1632.502}{X} - 178.205A + \frac{1485.708}{X^2} + 16.502A^2 + 328.302 \frac{A}{X} - \frac{445.855}{X^3} - 0.507A^3 - 15.449 \frac{A^4}{X} - 150.941 \frac{A}{X^2} + AX$$

(10)

For mixed beach (trench):

$$\frac{U}{u_{cb}} = 33.472 - 64.842X + 47.024X^2 - 18.41X^3 + 3.42X^4 - 0.241X^5 + 4.626A - 2.842A^2 + 0.9A^3 - 0.133A^4 + 0.0068A^5 + AX$$

(11)

For mixed beach (uniform slope):

$$\frac{U}{u_{cb}} = 0.533 + 3.881 \ln(X) - 1.553A - 10.534 \ln(X)^2 - 0.382A^2 + 3.182 \ln(X)A - 127.824 \ln(X)^3 + 0.481A^3 - 9.071 \ln(X)A^2 + 57.488 \ln(X)^2A + AX$$

(12)

where

U (cm/s) is the depth- and time-averaged undertow velocity with positive values for seaward direction,

u_{GB} (cm/s) is the value of the output of the model of Grasmeyer and Ruessink (2003),

X is the dimensional parameter which is equal to $\frac{D_i}{D_b}$, and

A is the dimensional parameter which is equal to $\frac{L_c}{h_i}$

The parameters D_i , D_b , D_t and h_i are shown in Fig. 22.

h_i (m) is the local water depth,

D_t (m) is the distance between the breaking point and the point of interest

D_b (m) is the distance from the point, where the local water depth is equal to the still water level, to the breaking point

D_i (m) is the distance from the point, where the local water depth is equal to the still water level, to the point of interest

The breaking depth for regular waves was calculated (Rattanapitikon and Shibayama, 2006) by

where,

$$h_b = (3.86m^2 - 1.98m + 0.88)H_0 \left(\frac{H_0}{L_0}\right)^{-0.16} \text{ for } \frac{H_0}{L_0} \leq 0.1 \quad (13a)$$

$$h_b = (3.86m^2 - 1.98m + 0.88)H_0 \left(\frac{H_0}{L_0}\right)^{-0.24} \text{ for } \frac{H_0}{L_0} > 0.1 \quad (13b)$$

and for random waves (Goda 1970,1985) by

$$H_b = AL_0 \left\{ 1 - \exp \left[-1.5 \frac{\pi d_b}{L_0} \left(1 + 15(\tan \beta)^{\frac{2}{3}} \right) \right] \right\} \quad (14)$$

where A = a coefficient (=0.12)

The breaking point is defined as the maximum wave height admissible for a given water depth (Torrini and Allsop, 1999).

The graphical presentations of the comparison of the experimental depth- and time-averaged undertow velocities results, for all Lines and all

tests, with the proposal equations (Eq. (5) to Eq. (12)) are shown in

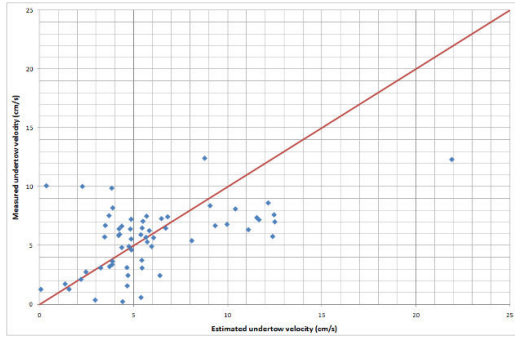


Fig.23 to

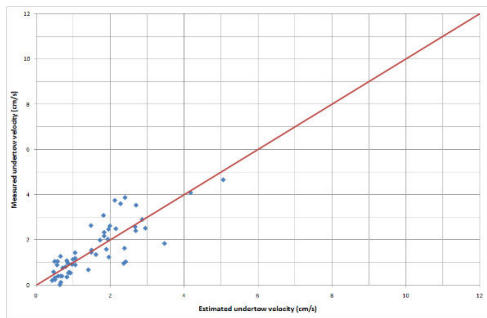


Fig.30 (the positive values represent the undertow velocities). In these figures, Eq. (5) to Eq. (12) show better agreement with the experimental data compared with the models of Kuriyama and Nakatsukasa (2000) and Grasmeijer and Ruessink (2003).

Discussion

The analysis of the cross-shore currents in both gravel and mixed beaches focused on the behaviour of the undertow and especially its behaviour near the bed. The undertow was observed in both trench and uniform slope for both types of beach. However, near the bed, the trench had higher values of undertow flow compare to the uniform slope beach and also had higher values with mixed beach compare to gravel beach. In addition, the velocities were higher at the gravel bed where the D_{50} was also the highest which was in agreement with the observation of Lara *et al.* (2002).

The cross-shore currents near the bed for both gravel and mixed beaches showed no reduction of their values and also showed an oscillated direction, from seaward to shoreward and from shoreward to seaward, along the cross-shore section of the beach. This behaviour including the case where the value of the cross-shore current velocity increased instead of being decreased can be caused from the permeability of the beach and also the mechanism of the bed-generated turbulence (Buffin-Bélanger *et al.*, 2000 and Shvidchenko *et al.*, 2001). This behaviour influenced the cross-shore sediment transport at the bed and it is more noticeable at gravel beach due to its higher permeability compare with mixed beach. The new empirical formulae estimated the undertow velocity by dividing the cross-section area based on the location of the point of interest and the breaking point compared to the local water depth. The new formulae estimated the undertow velocity more accurately than the the models of Kuriyama and Nakatsukasa (2000) and Grasmeijer and Ruessink (2003).

CONCLUSIONS

This paper investigated the behaviour of the undertow velocity on mixed and gravel beaches with uniform slope and a trench. New empirical formulae, based on the model of Grasmeijer and Ruessink (2003), were also proposed in order to predict time- and depth-averaged undertow velocity on mixed and gravel beaches. The new empirical formulae were based on a nonlinear regression of a modification of the Grasmeijer's and Ruessink's model where the zones where divided based on the related distance of the point of interest and the breaking point.

The formulae showed their accuracy, against other published equations, by comparing them with published data of large-scale experiment. The new formulae showed better results than the models of Kuriyama and Nakatsukasa (2000) and Grasmeijer and Ruessink (2003). The undertow velocity was estimated accurately.

ACKNOWLEDGEMENTS

The author would like to acknowledge the assistance and support provided by staff of Cardiff University and by staff of Franzius-Institute (Marienwerder) of University of Hannover for the completion of the physical model tests.

REFERENCES

- Antoniadis C., 2009. *Wave-induced currents and sediment transport on gravel and mixed beaches*. Ph.D. Thesis. Cardiff University, UK, 591 pp.
- Briand, M.-H., G., and Kamphuis J.W., 1993. Waves and currents on natural beaches: a quasi 3D numerical model. *J. of Coast. Eng.*, 20, 101-134.
- Buffin-Bélanger, T., Roy, A.G., Kirkbride, A.D., 2000. On large-scale flow structures in a gravel-bed river. *Geom.*, 32 (3-4), 417-435.
- Coastal Engineering Manual, 2003. *Surf zone hydrodynamics*. EM 1110-2-100, Part II, Chapter 4, US Army Corps. of Engineers, 40pp.
- Dally, W. R., and Dean, R. G. 1984. Suspended Sediment Transport and Beach Profile Evolution. *J. of Wat., Por., Coast., and Oc. Eng.*, 110 (1), 15-33.
- Deigaard, R., Justesen, P., Fredsoe, J., 1991. Modelling of undertow by a one-equation turbulence model. *Coastal Engineering*, 15, 431-458.
- Duncan, J.H., 1981. An Experimental Investigation of Breaking Waves Produced by a Towed Hydrofoil. p. 331-38. In: *Proc. R. Soc. Lond. A*, 377, 8 July 1981. RSP.
- Dyhr-Nielsen, M., and Sorensen, T., 1970. Some Sand Transport Phenomena on Coasts with Bars. p.1993-2004. In: *Proceedings of the 12th Coastal Engineering Conference*, American Society of Civil Engineers.
- Engelund, 1981. F. Engelund, A simple theory of weak hydraulic jumps. p.29-31. In: *Progress Report No. 54*, Institute of Hydrodynamics and Hydraulic Engineering, ISVA, Technical University Denmark, 1981.
- Grasmeijer, B.T., and Uesink, B.G., 2003. Modelling of waves and currents in the nearshore parametric vs. Probabilistic approach. *J. of Coast. Eng.*, 49, 185-207.
- Goda, Y., 1970. A synthesis of breaker indices. *Trans. JSCE*, 2, 227-230.
- Goda, Y., 1983. *A unified nonlinearity parameter of water waves*. Report of Port Harbour Res. Inst., 22 (3), 3-30.
- Goda, Y., 1985. *Random Seas and Design of Maritime Structures*. University of Tokyo Press., ISBN 0-86008-369-1, Tokyo, 464pp.
- Hansen, J. B., and Svendsen, I. A., 1984. A Theoretical and Experimental Study of Undertow. p.2246-2262. In: *Proceedings of the 19th Coastal Engineering Conference*, American Society of Civil Engineers.
- Kuriyama, Y., 1996. Models of wave height and fraction of breaking waves on a barred beach. p.247-260. In: *Proc. 25th Coastal Eng. Conf.*, ASCE.
- Kuriyama, Y., and Ozaki, Y., 1996. *Wave height and fraction of breaking waves on a bar-trough beach – field measurements at HORS and modelling*. Report Port Harbour Res. Inst., 35 (1), 1-38.
- Kuriyama, Y., and Nakatsukasa, T., 2000. A one-dimensional model for undertow and longshore current on a barred beach. *Journal of Coastal Engineering*, 40, 39-58.
- Lara, J.L., Losada, I.J., Cowen, E.A., 2002. Large-scale turbulence structures over an immobile gravel-bed inside the surf zone. p. 1050-1061. In: *Smith, J.M. (Ed.), 28th International Conference on Coastal Engineering*, WS, Cardiff, UK.
- Madsen, P.A., Sørensen, O.R., Schaffer, H.A., 1997. Surf zone dynamics simulated by a Boussinesq type model: Part I. Model description and crossshore motion of regular waves. *Coast. Eng.*, 32, 255-287.
- Pedrono-Acuna, A., Simmonds, D.J., Otta, A.K., Chadwick, A.J., 2006. On the cross-shore profile change of gravel

- beaches. *Journal of Coastal Engineering*, 53, 335-347.
- Rattanapitikon, W., and Shibayama, T., 2006. Breaking wave formulas for breaking depth and orbital to phase velocity ratio. *Coast. Eng. J.*, 48 (4), 395-416.
- Seyama, A., and Kimura, A., 1988. The measured properties of irregular wave breaking and wave height change after breaking on the slope. p.419-432. In: *Proc. 21st Coastal Eng. Conf.*, ASCE.
- Shvidchenko, A.B., Pender, G., Hoey, T.B., 2001. Critical shear stress for incipient motion of sand/gravel streambeds. *Water Resources Research*, 37, 2273-2284.
- Stive, M. J. F., and Wind, H. F. 1986. Cross-shore Mean Flow in the Surf Zone. *Coastal Engineering*, 10 (4), 325-340.
- Svendsen, I.A., 1984a. Mass flux and undertow in a surf zone. *Coastal Engineering*, 8, 347-365
- Svendsen, I.A., 1984b. Wave heights and set-up in a surf zone. *Coastal Engineering*, 8, 303-329.
- Svendsen, I. A., Schäffer, H. A., Hansen, J. B. 1987. The Interaction Between the Undertow and the Boundary Layer Flow on a Beach. *J. of Geoph. Res.*, 92 (C11), 11845-11856.
- Svendsen, I.A. and Buhr Hansen, J., 1988. Cross-shore currents in surf zone modelling. *Coastal Eng.*, 12: 23-42, 11845-11856.
- Svendsen, IB. A., and Lorenz, R.S., 1989. Velocities in combined undertow and longshore currents. *Coast. Eng.*, 13, 55-79.
- Tajima, Y., and Madsen, O. S., 2002. Shoaling, breaking and broken wave characteristics. p.222-234. In: *Proc., 28th Int. Conf. on Coastal Engineering*, ASCE, Reston, Va..
- Tajima, Y., and Madsen, O. S., 2003. Modeling near-shore waves and surface rollers. In: *Proc., 2nd Int. Conf. on Asian and Pacific Coasts_CD-ROM_*, World Scientific, Singapore, ISBN 981-238-558-4.
- Tajima, Y., and Madsen, O. S., 2006. Modeling near-shore waves, surface rollers, and undertow velocity profiles. *Journal of Waterway, Port, Coastal, and Ocean Engineering*, 132(6), 429-438.
- Ting, F.C.K., and Kirby, J.T., 1994. Observation of undertow and turbulence in a laboratory surf zone. *Coastal Engineering*, 24, 51-80.
- Torrini, L., and Allsop, N.W.H., 1999. Goda's breaking prediction method- A discussion note on how this should be applied. *HR Report, IT 473*, Wallingford, U.K.
- Visser, P. J., 1991. Laboratory Measurements of Uniform Longshore Currents. *Coast. Eng.*, 15(5), 563-593.

Appendix A

Observation of the cross-shore currents, of each individual test and line, during the experiment

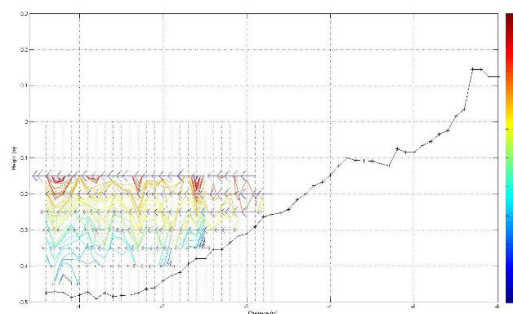


Fig. A.1: 2D presentation of the time-averaged currents (cm/s) for Test 1-Line 1

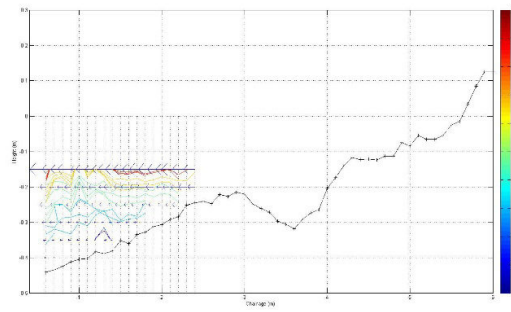


Fig. A.2:2D presentation of the time-averaged currents (cm/s) for Test 1- Line 2

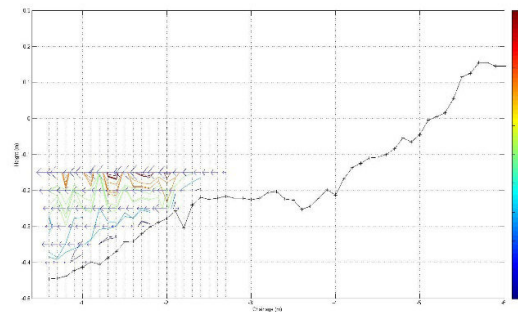


Fig. A.3:2D presentation of the time-averaged currents (cm/s) for Test 1- Line 3

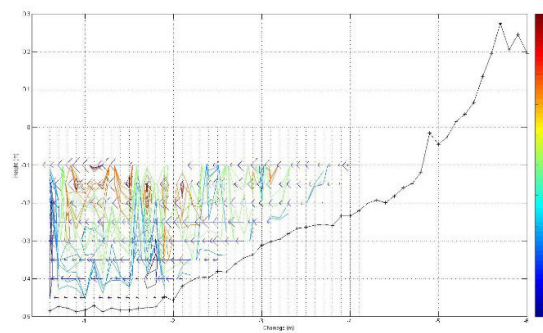


Fig. A.4:2D presentation of the time-averaged currents (cm/s) for Test 2- Line 1

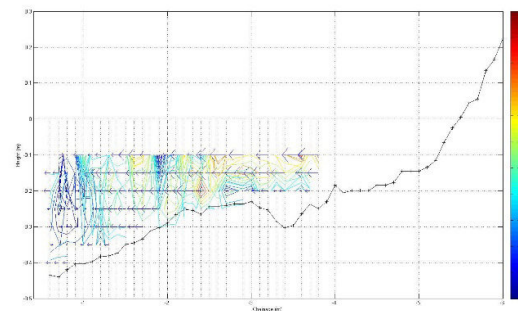


Fig. A.5:2D presentation of the time-averaged currents (cm/s) for Test 2- Line 2

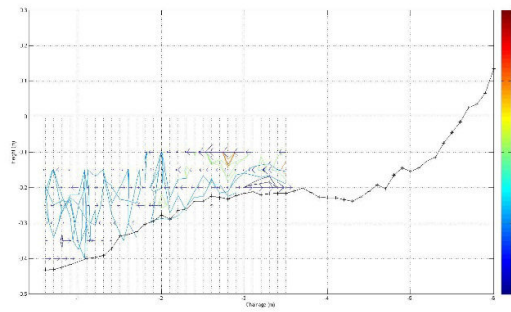


Fig. A.6: 2D presentation of the time-averaged currents (cm/s) for Test 2- Line 3

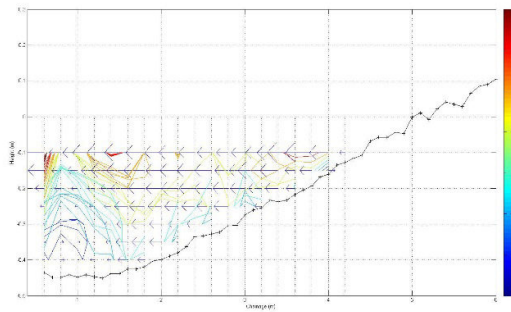


Fig. A.7: 2D presentation of the time-averaged currents (cm/s) for Test 3- Line 1

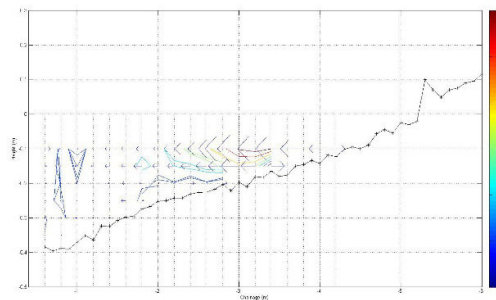


Fig. A.8: 2D presentation of the time-averaged currents (cm/s) for Test 3- Line 2

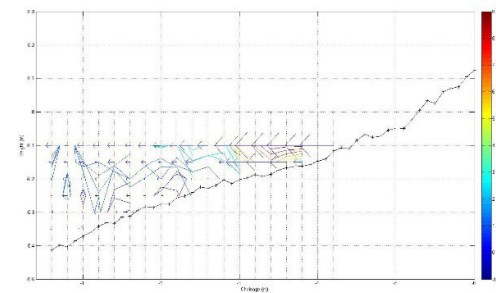


Fig. A.9: 2D presentation of the time-averaged currents (cm/s) for Test 3- Line 3

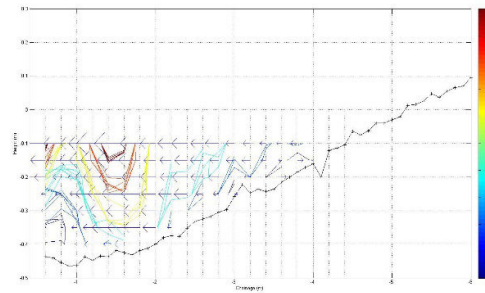


Fig. A.10:2D presentation of the time-averaged currents (cm/s) for Test 4- Line 1

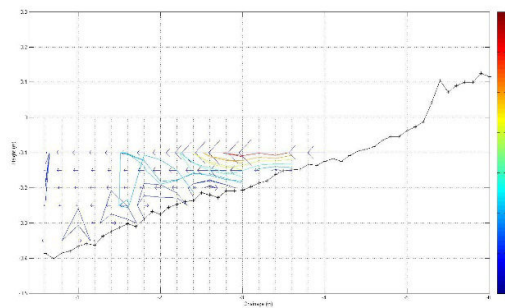


Fig. A.11:2D presentation of the time-averaged currents (cm/s) for Test 4- Line 2

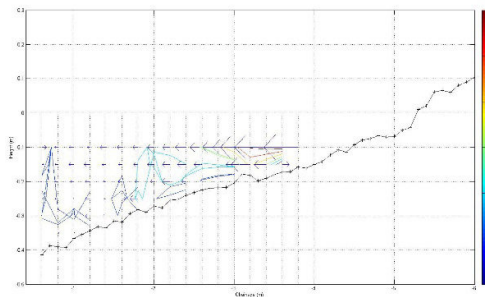


Fig. A.12:2D presentation of the time-averaged currents (cm/s) for Test 4- Line 3

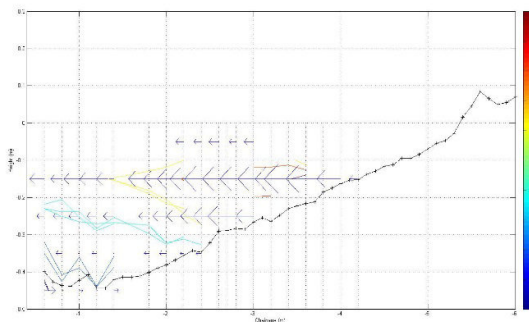


Fig. A.13:2D presentation of the time-averaged currents (cm/s) for Test 5- Line 1

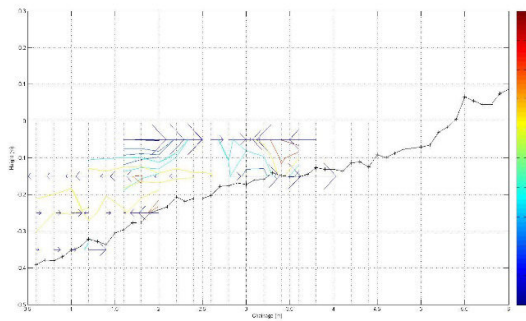


Fig. A.14:2D presentation of the time-averaged currents (cm/s) for Test 5- Line 2

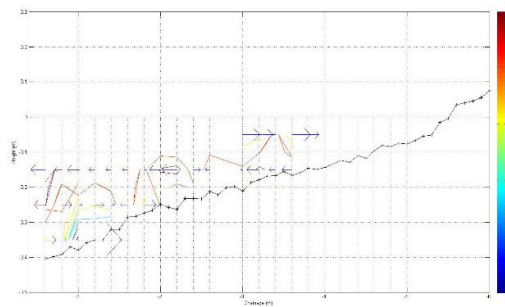


Fig. A.15:2D presentation of the time-averaged currents (cm/s) for Test 5- Line 3

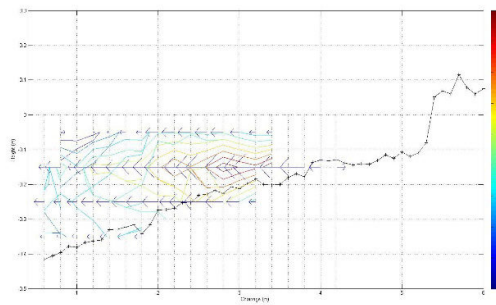


Fig. A.16:2D presentation of the time-averaged currents (cm/s) for Test 6- Line 1

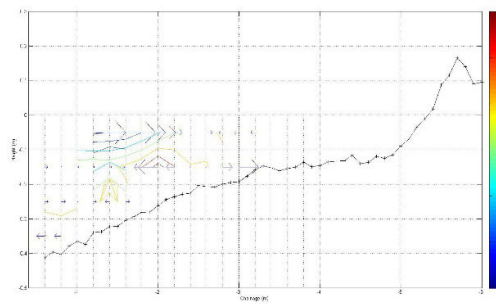


Fig. A.17:2D presentation of the time-averaged currents (cm/s) for Test 6- Line 2

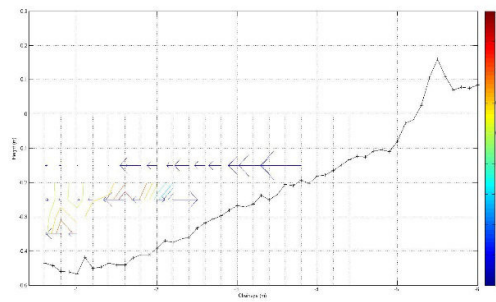


Fig. A.18:2D presentation of the time-averaged currents (cm/s) for Test 6- Line 3

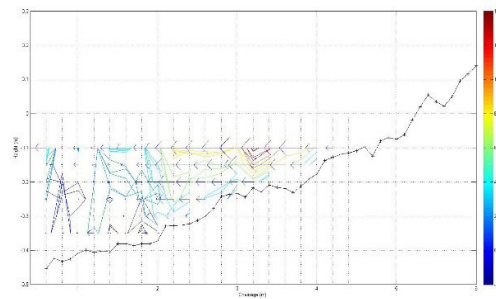


Fig. A.19:2D presentation of the time-averaged currents (cm/s) for Test 7- Line 1

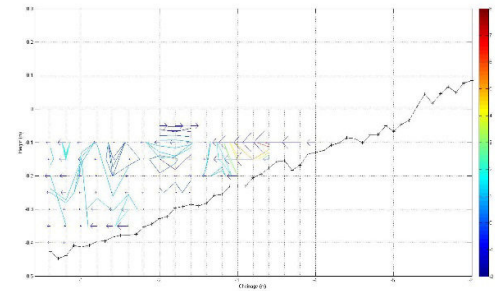


Fig. A.20:2D presentation of the time-averaged currents (cm/s) for Test 7- Line 2

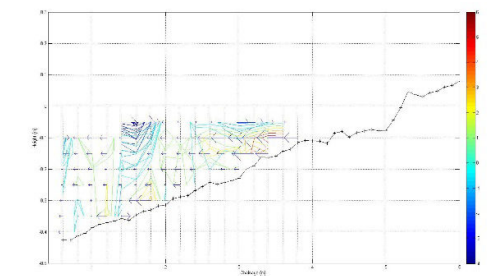


Fig. A.21:2D presentation of the time-averaged currents (cm/s) for Test 7- Line 3

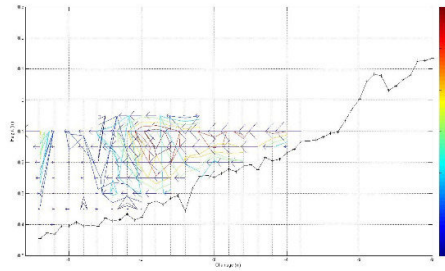


Fig. A.22:2D presentation of the time-averaged currents (cm/s) for Test 8- Line 1

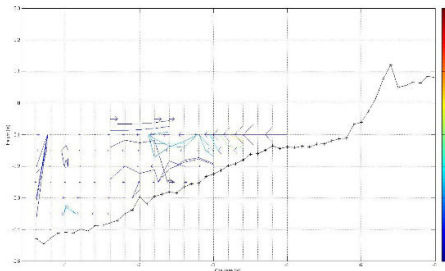


Fig. A.23:2D presentation of the time-averaged currents (cm/s) for Test 8- Line 2

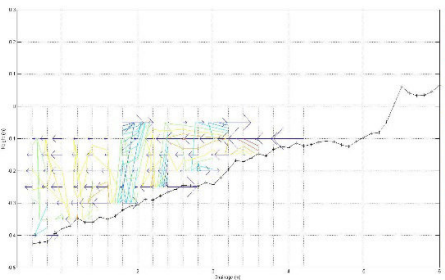


Fig. A.24:2D presentation of the time-averaged currents (cm/s) for Test 8- Line 3

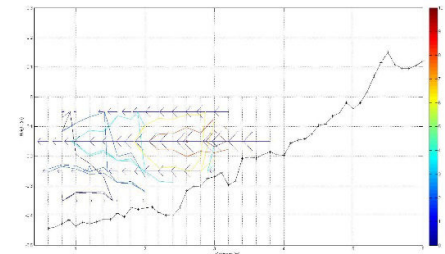


Fig. A.25:2D presentation of the time-averaged currents (cm/s) for Test 9- Line 1

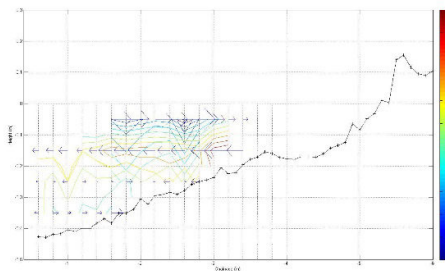


Fig. A.26: 2D presentation of the time-averaged currents (cm/s) for Test 9- Line 2

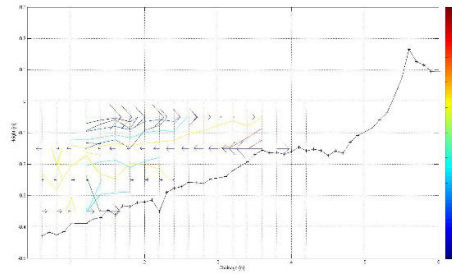


Fig. A.27: 2D presentation of the time-averaged currents (cm/s) for Test 9- Line 3

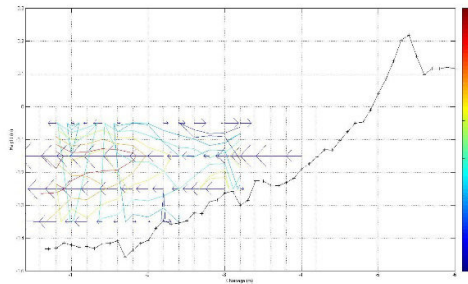


Fig. A.28: 2D presentation of the time-averaged currents (cm/s) for Test 10- Line 1

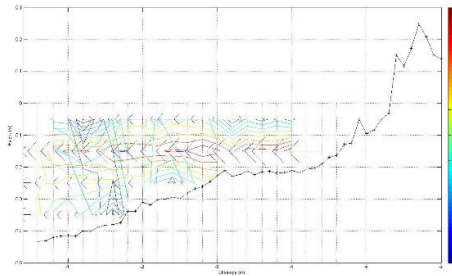


Fig. A.29: 2D presentation of the time-averaged currents (cm/s) for Test 10- Line 2

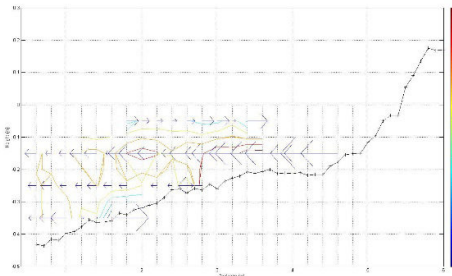


Fig. A.30: 2D presentation of the time-averaged currents (cm/s) for Test 10- Line 3

Appendix B

The undertow model of Kuriyama and Nakatsukasa (2000)

The time- and depth-averaged undertow velocity of an individual wave V_{ind} is estimated

with the volume flux due to the organised wave motion Q_w and that due to the surface roller Q_r .

$$V_{ind} = -\frac{(Q_w + Q_r)}{d_{tr}} \quad (B.1)$$

where d_{tr} is the distance between the wave trough level and the bottom, and is simply determined as

$$d_{tr} = h - \frac{H}{4} \quad (B.2)$$

where h is the water depth and H is the wave height. For random waves H is represented by H_{m0} .

The volume flux due to the organized wave motion Q_w is calculated with the wave celerity C , the water depth h , and the root-mean-square of water surface elevation of an

individual wave ζ_{rms} by the following equation proposed by Svendsen (1984a):

$$Q_w = - \left(\frac{L}{h} \right) \zeta_{rms}^2 \quad (B.3)$$

The value of ζ_{rms} is estimated with consideration for the wave nonlinearity. With the parameter Π expressing nonlinearity of an individual wave and experimental data shown by Goda (1983), the relationship between ζ_{rms} and H was obtained; the parameter Π and the relationship obtained are expressed by:

$$\Pi = \frac{H}{L \cot h^2 \left(\frac{2\pi h}{L} \right)} \quad (B.4)$$

$$\zeta_{rms} = \begin{cases} \frac{1}{2\sqrt{2}} H, & \Pi < 0.15, \\ \frac{1}{1.668 \log \Pi + 4.204} H, & 0.15 \leq \Pi \leq 3, \\ \frac{1}{5} H, & \Pi \geq 3. \end{cases} \quad (B.5)$$

In the estimation of Q_r , the volume flux due to the roller is obtained from

$$Q_r = - \frac{A_r \ell}{2L} \quad (B.6)$$

where A_r is the area of the roller. The area of the surface roller is estimated on the basis of the assumptions mentioned below.

The area of the surface roller is basically assumed to be proportional to the square of the wave height. The area A_{r1} is estimated with a dimensionless coefficient C_A from

$$A_{r1} = C_A H^2 \quad (B.7)$$

where C_A is given by

$$\frac{H_b}{h_b} = C_{Dr} \left[\frac{0.16 \frac{L_0}{h_b} \left[1 - \exp \left\{ -0.8\pi \frac{h_b}{L_0} \left(1 + 15 \tan^2 \beta \right) \right\} \right]}{0.96 \tan \beta + 0.2} \right] \quad (B.10)$$

For regular waves (Seyama and Kimura, 1988):

$$H_b = 1.25 h_b \left[\frac{0.16 \frac{L_0}{h_b} \left[1 - \exp \left\{ -0.8\pi \frac{h_b}{L_0} \left(1 + 15 \tan^2 \beta \right) \right\} \right]}{0.96 \tan \beta + 0.2} \right] \quad (B.11)$$

$$C_A = 17.0 \log \xi_b + 24.7 \quad (B.8)$$

where ξ_b is the surf similarity parameter at the wave breaking position and is estimated by

$$\xi_b = \frac{\tan \beta}{\sqrt{\left(\frac{H_{1/3,b}}{L_{1/3,0}} \right)}} \quad (B.9)$$

where $\tan \beta$ is the bed slope, $L_{1/3,0}$ is the offshore wavelength corresponding to the significant wave period and $H_{1/3,b}$ is the significant wave height at the wave-breaking position and is estimated by:

For random waves (Kuriyama, 1996):

where H_b is the wave breaking height, h_b is the wave breaking depth and L_0 is the wavelength in deep water. C_{br} is a dimensionless coefficient with a range from 0.7 to 1.2.

The energy of the surface roller should not exceed the energy transferred from the

organized wave motion. The roller area is therefore determined not to exceed the roller area A_{r2} estimated without the energy dissipation of the surface roller from the following equation:

$$\frac{\partial(E_w C_g)}{\partial y} + \frac{\partial(W_r C_g)}{\partial y} = 0 \quad (B.12)$$

where,

$$W_r = \frac{1}{8} \rho C^2 \frac{A_{r2}}{L} \quad (B.13)$$

$$\frac{\partial(E_w C_g)}{\partial y} = \frac{1}{4} \rho g \frac{1}{T} \frac{(BH)^3}{h} \quad (B.14)$$

where W_r is the energy of the roller having the distribution of the time-averaged velocity above the wave trough level, E_w is the energy of the organized wave motion ($=\rho g H^2/8$), C_g is the group velocity, ρ is the sea water density, T is the wave period, H is the wave height, h is

the water depth, and B is a dimensionless coefficient determining the amount of energy dissipation. Kuriyama and Ozaki (1996) investigated the coefficient B with the experimental data of Seyama and Kimura (1988), and proposed the following formula:

$$B = C_B \left\{ 1.6 - 0.12 \ln \left(\frac{H_b}{L_0} \right) + 0.28 \ln(\tan \beta) \right\} \quad (B.15)$$

where H_0 is the wave height in deep water, and C_B is a dimensionless coefficient with a range from 0.7 to 1.1.

The surface roller diminishes at the wave reforming point.

In the actual calculation, A_{r1} and A_{r2} are estimated and the smaller value is assumed to be the area of the surface roller.

Appendix C

The undertow model of Grasmeyer and Ruessink (2003)

The time- and depth-averaged undertow velocity \bar{u} is derived from the mass flux due to the wave motion (Q_w) and the mass flux due to the surface roller (Q_r).

$$\bar{u} = - \frac{(Q_w + Q_r)}{h_{trough}} \quad (C.1)$$

where $h_{trough} = h - H/2$

where h is the water depth and H is the wave height. For random waves H is represented by H_{rms} .

Using linear theory, Q_w is computed as

$$Q_w = \frac{E}{\rho c} = \frac{1}{8} \left(\frac{E}{\rho c} \right) H^2 \cos \theta \quad (C.2)$$

where E is the wave energy ($=\cos\theta\rho g H^2/8$) for obliquely waves, θ is the angle of incidence, ρ is the density of the water and c is the wave phase speed.

The roller distribution Q_r is computed as (Svendsen, 1984a)

$$Q_r = \frac{A}{T} = \frac{2E_r}{\rho c} \cos \theta \quad (C.3)$$

where A is the roller area, T is the wave period and E_r is the roller energy density and is estimated by

$$E_r = \frac{\rho A c^2}{2L} = \frac{\rho A c}{2T} \quad (C.4)$$

Figures

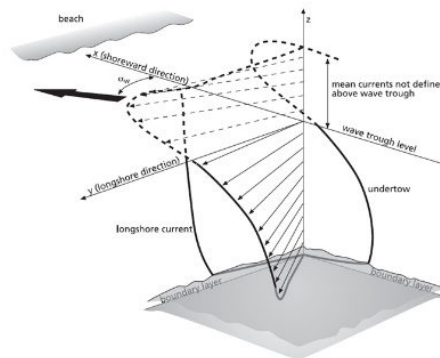


Fig. 1: Schematic diagram of the vertical profile of the mean cross-shore and longshore current in the nearshore

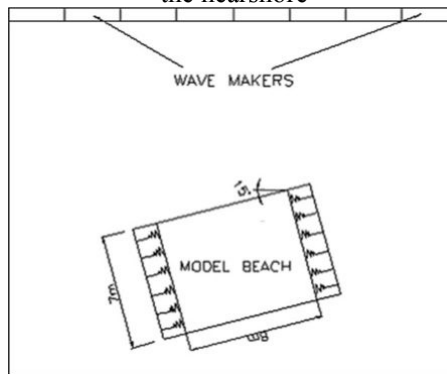


Fig. 2: Position of the beach model

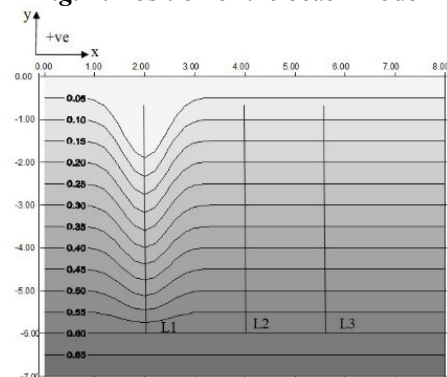


Fig. 3: Model bathymetry (trench, uniform slope) and location of measurements

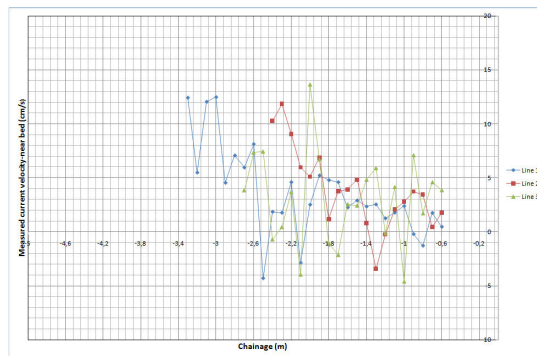


Fig. 4: Near bed cross-shore current velocity (Test 1)

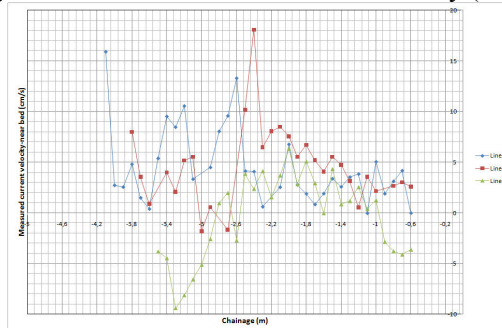


Fig. 5: Near bed cross-shore current velocity (Test 2)

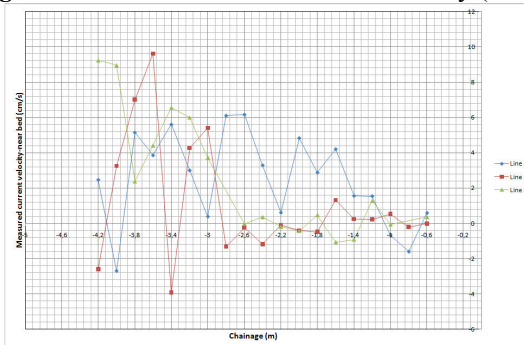


Fig. 6: Near bed cross-shore current velocity (Test 3)

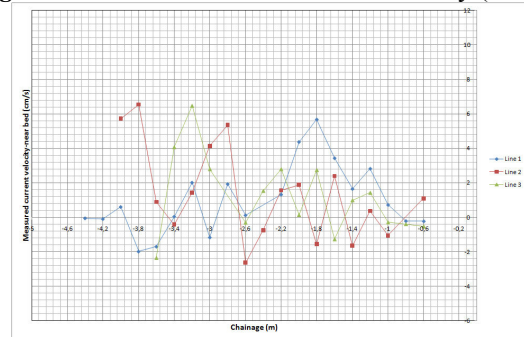


Fig. 7: Near bed cross-shore current velocity (Test 4)

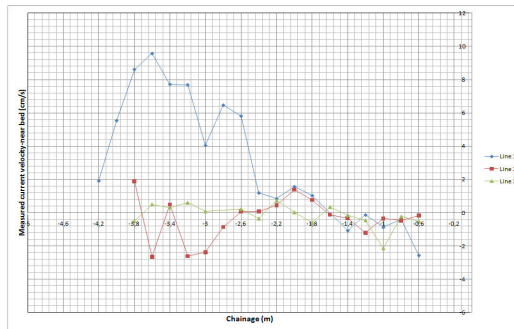


Fig. 8: Near bed cross-shore current velocity (Test 5)

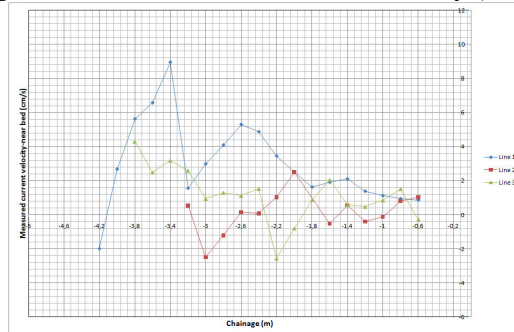


Fig. 9: Near bed cross-shore current velocity (Test 6)

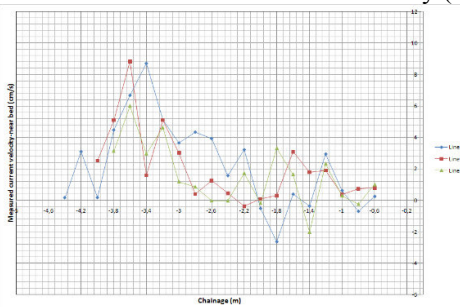


Fig. 10: Near bed cross-shore current velocity (Test 7)

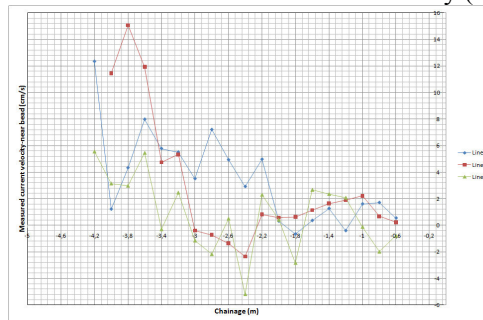


Fig. 11: Near bed cross-shore current velocity (Test 8)

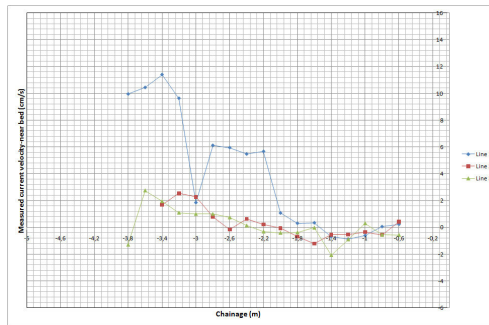


Fig. 12: Near bed cross-shore current velocity (Test 9)

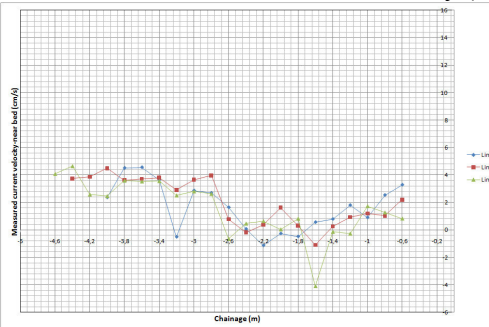


Fig. 13: Near bed cross-shore current velocity (Test 10)

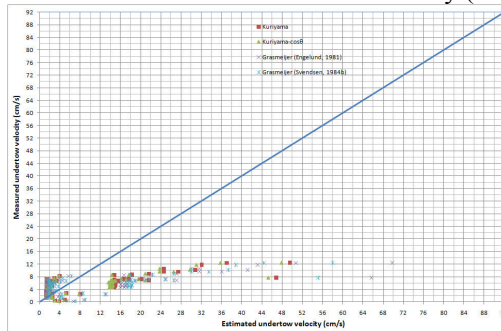


Fig. 14: Estimated vs. Measured undertow velocity (Regular waves/gravel beach - trench)

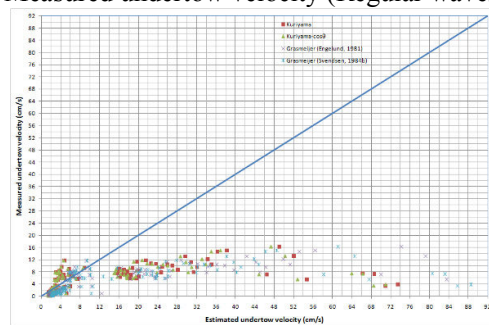


Fig. 15: Estimated vs. Measured undertow velocity (Regular waves/gravel beach- uniform slope)

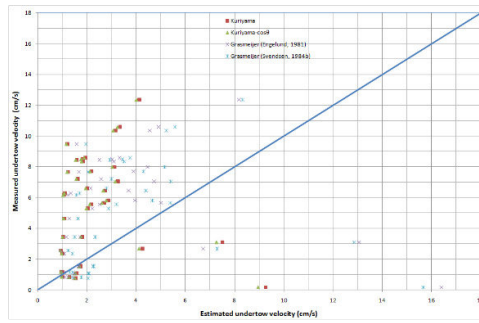


Fig. 16: Estimated vs. Measured undertow velocity (Regular waves/mixed beach- trench)

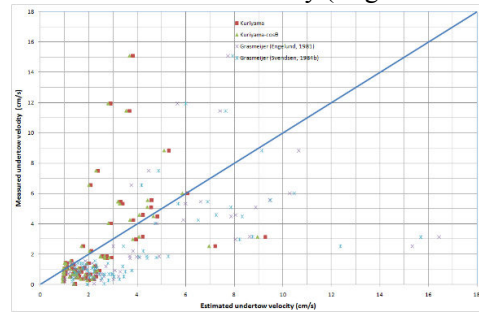


Fig. 17: Estimated vs. Measured undertow velocity (Regular waves/mixed beach- uniform slope)

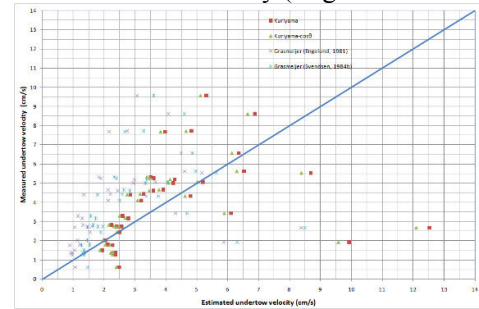


Fig. 18: Estimated vs. Measured undertow velocity (Random waves/gravel beach- trench)

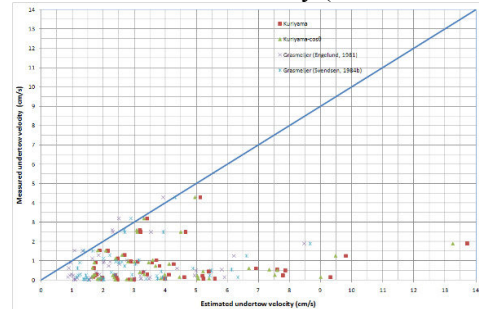


Fig. 19: Estimated vs. Measured undertow velocity (Random waves/gravel beach- uniform slope)

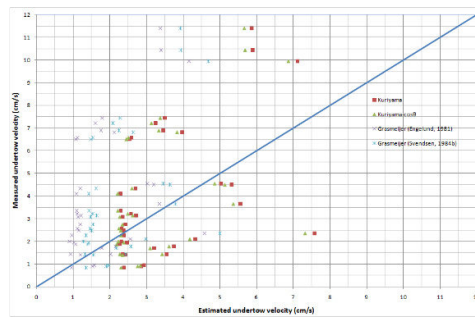


Fig. 20: Estimated vs. Measured undertow velocity (Random waves/mixed beach- trench)

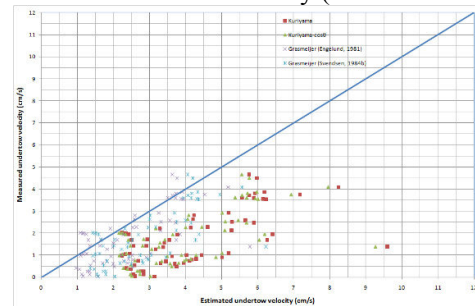


Fig. 21: Estimated vs. Measured undertow velocity (Random waves/mixed beach- uniform slope)

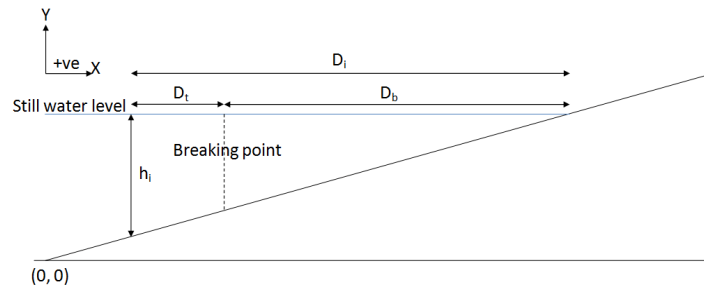


Fig. 22: Schematisation of the components of A and X

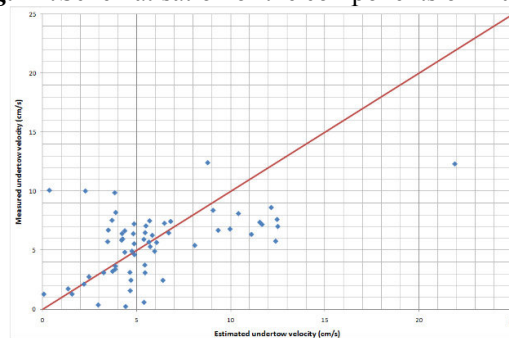


Fig. 23: Estimated vs. Measured undertow velocity (Regular waves/gravel beach - trench)

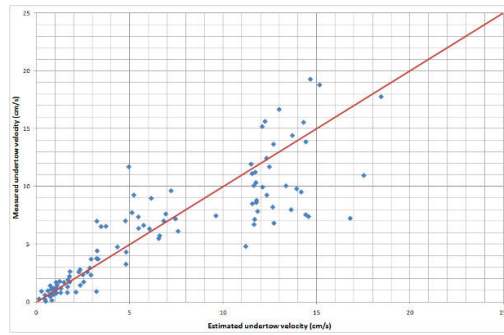


Fig.24:Estimated vs. Measured undertow velocity (Regular waves/gravel beach – uniform slope)

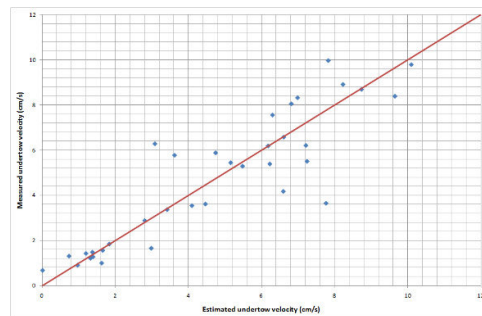


Fig.25:Estimated vs. Measured undertow velocity (Regular waves/Mixed Beach - trench)

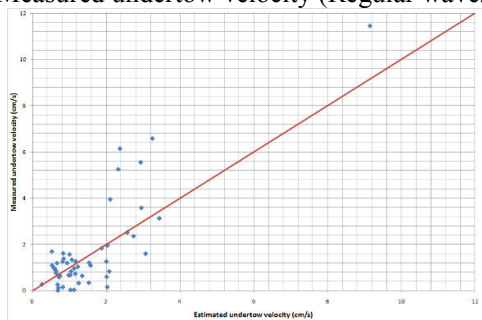


Fig.26:Estimated vs. Measured undertow velocity (Regular waves/Mixed Beach – uniform slope)

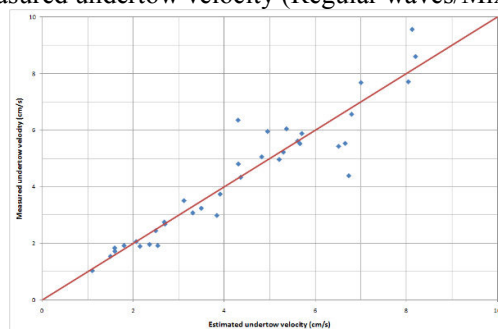


Fig.27:Estimated vs. Measured undertow velocity (Random waves/gravel beach - trench)

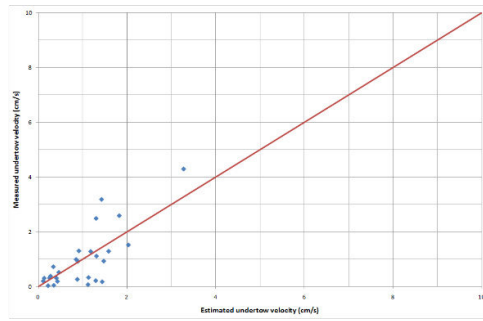


Fig.28: Estimated vs. Measured undertow velocity (Random waves/gravel beach – uniform slope)

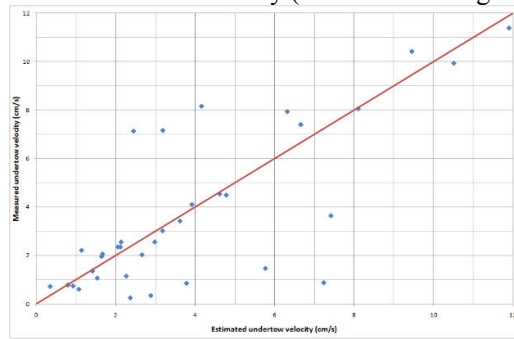


Fig.29: Estimated vs. Measured undertow velocity (Random waves/Mixed Beach - trench)

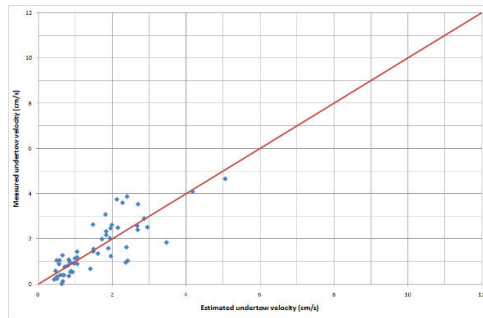


Fig.30: Estimated vs. Measured undertow velocity (Random waves/Mixed Beach – uniform slope)

Tables

Table 1. The different particle sizes of the sediments

Type of Beach	D ₅ (mm)	D ₁₅ (mm)	D ₁₆ (mm)	D ₅₀ (mm)	D ₈₄ (mm)	D ₈₅ (mm)	D ₉₀ (mm)	D ₉₄ (mm)
Gravel Beach (G)	15.35	16.66	16.83	22.76	28.38	28.86	29.59	30.50
Mixed Beach (M)	0.21	0.32	0.33	12	25.20	25.9	27.31	29.19

Table 2. Test programme of the experiments

TESTS (Regular Waves)	Wave Height (H)	Wave Period (T)	TESTS (Random Waves)	Significant Wave Height (H _{m0})	Spectral Peak Period (T _p)
Test 1-G	25.3 cm	2 sec	Test 5-G	10.8 cm	2.3 sec
Test 2-G	21.8 cm	3 sec	Test 6-G	11 cm	3.2 sec

Test 3-G	8.6 cm	2 sec	Test 9-M	11 cm	2.3 sec
Test 4-G	9.2 cm	3 sec	Test 10-M	11.7 cm	3.1 sec
Test 7-M	8.6 cm	2 sec			
Test 8-M	7.7 cm	3 sec			